

Heating-Rate and Particle-Size Effects on Melting Process of Au Nanoparticles

Jixing Chen, Xiaofeng Fan,* Jialin Liu, Changzhi Gu, Yunfeng Shi, David J. Singh, and Weitao Zheng

Cite This: *J. Phys. Chem. C* 2020, 124, 7414–7420

Read Online

ACCESS |



Metrics & More

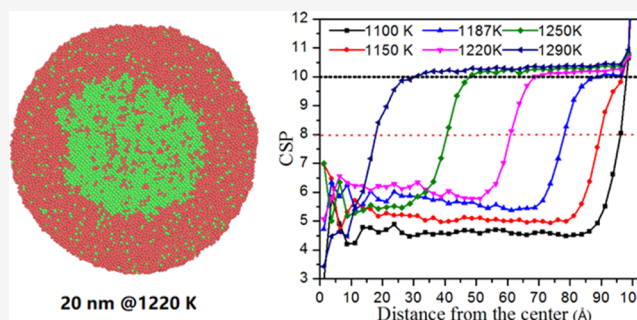


Article Recommendations



Supporting Information

ABSTRACT: The atomic mechanisms of the melting process of gold nanoparticles were investigated by molecular dynamics simulations. Melting under a high heating rate is found to be much different from the near equilibrium melting and is a typical overheating process. The melting begins with the formation of a premelting layer near the surface, and the interface of the solid and premelting layer drives the nucleation of the liquid into the interior of nanoparticles. The high heating rate causes solid–liquid coexistence in a large temperature interval. These imply that the melting process can be controlled effectively by different heating ways.



INTRODUCTION

Metallic nanoparticles are of particular interest due to their broad application areas, including industrial catalysis, medicine, and optoelectronic devices.¹ Metallic nanoparticles have properties different from their bulk counterparts. These include localized surface plasmons, enhanced catalytic activity, and Raman scattering enhancement due to the localized electric field. A fundamental understanding of their thermodynamic properties, such as melting process and temperature, is important especially for high-temperature applications, including high-temperature catalysis.² In fact, there exists a body of research on the thermodynamic properties of nanoparticles.^{3–9} It is established that metal nanostructures generally have depressed melting temperature relative to bulk and that the melting temperature decreases with decreasing particle size. However, the underlying melting mechanisms of nanoparticles are less understood.

Au nanoparticles have been regarded as a representative model system. As such, their thermodynamic properties have been studied for many years. In the previous experimental research of Buffat and Borel,¹⁰ the melting points of gold nanoparticles were found to be depressed with decreasing size as anticipated. However, the melting temperature does not vary near linearly with the reciprocal of size in the range of 2–22 nm. Meanwhile, theoretical studies were performed in efforts to elucidate the melting mechanism. In a perfect crystalline metal, there is homogeneous melting aided by thermal fluctuations in the absence of preferential nucleation sites.¹¹ The nucleation of liquid is usually initiated under sufficient superheating above the melting point.^{12,13} In the actual melting process of metals, melting is initiated at surface or at crystal defects.^{14,15} It means the existence, quantity, and nature of the surfaces and/or defects determine the melting

process. For nanoparticles, melting has been proposed to initiate from surfaces. This is motivated by the idea that in general the surface atoms are less well bonded than bulk atoms and have higher energy, making them more likely to be mobile at a given temperature.^{16,17} Then, the interface between solid and liquid sweeps quickly through the solid core from the surface under continuous heating.

Several theoretical models were proposed to describe the size dependence of the melting process and the melting temperature. These include the Pawlow model,¹⁸ Rie model,¹⁹ and Reiss–Wilson model²⁰ with more recent discussion and developments by Xue et al.,²¹ Cui et al.,²² Fu et al.,²³ and Dai et al.²⁴ These theoretical models explain the experimental observations with suitable parameters and make predictions. An important one is the linear dependency of melting temperature on the inverse particle size in most cases over a range of not too small particle size. These models generally fail to predict the melting temperature of very small particles with size less than 5 nm. Experiments in this size range are often difficult. In these regards, molecular dynamics (MD) simulations can play an important role in analyzing the melting temperature and in exploring the changes of structures in the dynamic process of melting. Lewis et al.²⁵ carried out MD simulations to study the melting of unsupported gold nanoclusters within 1.6–5.1 nm. Shim et al.²⁶ investigated the

Received: November 18, 2019

Revised: March 10, 2020

Published: March 10, 2020

thermal stability of unsupported gold nanoparticles within 1.6–6 nm. Koga et al.²⁷ found that gold nanoparticles over a wide size range of 3–14 nm undergo a structural transformation from icosahedral to decahedral morphology just below the melting point. Qiao et al.²⁸ employed MD simulations to study the melting of gold nanoparticles with 2.5–5.3 nm. Dai et al.²⁴ simulated the premelting phenomena in gold nanoparticles with sizes of 8, 10, and 12 nm. There is also a body of work on Au clusters.^{29–31} All of these studies on smaller particles show that the melting process for gold nanoparticles begins with surface premelting.

Turning to experiments, Schlexer et al.³² very recently used high-resolution transmission electron microscopy on nanoparticles with size less than 10 nm combined with MD simulations to confirm the linear dependence of melting temperature on inverse particle size. Although a lot of simulation work has been done, the exploration of detailed kinetic melting processes is still lacking, especially for relatively large nanoparticles at reasonably high heating rates. High heating rates are increasingly of interest due to advances in experimental observation under these conditions with laser or electron beam heating. In addition, they can be relevant to developing technologies such as certain types of additive manufacturing.³³

Here, we reported MD simulations on unsupported spherical Au nanoparticles with diameters in the range 6–24 nm to explore the melting process. The changes of atomic structures near melting point were analyzed by the polyhedral template matching (PTM)³⁴ and the centrosymmetry parameter (CSP).³⁵ We found that the melting of these nanoparticles was a process with the coexistence of solid and liquid over a large range of temperature under a high heating rate, in addition to the surface premelting. The width of liquid region increased continually with temperature far from the melting point. Furthermore, we found that with the increase of particle size and with increase of heating rate, the range of melting temperature became larger.

COMPUTATIONAL METHODS

The large-scale atomic/molecular massively parallel simulator³⁶ was used to perform the MD simulations reported here. The interactions were modeled in the embedded-atom method (EAM). This consists of a pairwise potential and a many-body embedding energy with the formula

$$E_c = \sum_i c_i \left(\sum_{i \neq j} \rho_j(r_{ij}) \right) + \frac{1}{2} \sum_{i,j(i \neq j)} u_{ij}(r_{ij}) \quad (1)$$

where c_i is the embedding energy of atom i , ρ_j is the spherically averaged atomic density, and u_{ij} is the sum over atom pairs. Here, the EAM potential of gold is the form proposed by Foiles et al.³⁷ This potential predicts the properties of gold well, including equilibrium lattice constants, bulk modulus, elastic constants, sublimation energy, and formation energy of single vacancy. The atomistic configurations were visualized by the structure identification software, OVITO.³⁸ The simulation time step was set to 1 fs.

Particle sizes in the range 6–24 nm were investigated. This corresponds to between 6689 and 542,788 atoms. We started with face-centered cubic (fcc) gold and lattice parameter of 4.078 Å, which was consistent with bulk Au. In small nanoparticles (size less than 5 nm), the atoms are usually

arranged as a fcc-truncated Marks decahedra. Although the smaller particles possibly have different morphology, such as the icosahedral and decahedral, the morphology of larger particles generally is taken as spherical. Here, we use this as the initial structure, with particles constructed by removing atoms outside a specified radius while keeping free boundary conditions. Before the heating, all systems were relaxed at 300 K for 20 ps to reach the steady state. Then, a continuous heating process was imposed with a constant heating rate.

The heating rate was set to 1 K/ps.³³ The melting temperature of bulk gold was found to be 1372 K, based on the model potential. This is consistent with the experimental value 1337 K, especially if some overheating due to the rapid heating is considered. We also considered different heating rates, including 3, 2, 0.5, and 0.1 K/ps, as well as stepwise heating to explore effect of heating rate on the melting process. The simulations were performed in the NVT ensemble with the temperature maintained using Nosé–Hoover thermostats.³⁹

The phase transition from solid to liquid can be identified using the average potential energy as a function of temperature. Under isobaric condition, the heat capacity is the first derivative of enthalpy with respect to temperature. In vacuum or normal atmospheric pressure, the P_V term in enthalpy can be ignored and the heat capacity can be expressed as $C_V = \partial E_p / \partial T + \frac{3}{2} k_B$, where k_B is Boltzmann constant and E_p is the potential energy. The melting point for bulk can be decided unambiguously. However, melting is a process over a range of temperatures for nanoparticles.

RESULTS AND DISCUSSION

The Lindemann index is a typical indicator to analyze the melting from solid to liquid and can decide the melting temperature with a critical ratio, such as $\delta_L = 0.22$ for single crystal gold.⁴⁰ In the single crystal, melting is initialized when the Lindemann stability criteria of randomly localized atoms is exceeded. For nanoparticles, surface premelting has been widely accepted and investigated extensively. The surface premelting is mainly due to vacancies around the surface atoms or/and the under-coordination of surface atoms with surface lattice softening or surface phonon instabilities. The high amplitude of the resulting thermal vibrations results in surface atoms and atoms near the surface, satisfying the Lindemann instability criteria at temperatures well below the bulk melting temperature. Related to this, we noticed that the work of Dai et al.²⁴ indicated that surfaces on different crystal directions could have significantly different premelting widths, for example, under certain conditions 1.1 nm in the [100] and [110] directions and 0.45 nm in the [111] direction.

We observe that the coexistence of solid and liquid is common at a high heating rate in larger nanoparticles. This is in addition to the phenomenon of premelting in smaller particles under a slow heating rate (verified by step-by-step heating simulations). As shown in Figure 1, with a particle size of 20 nm, as an example, melting becomes a continuous process that occurs over a large range of temperature. The atomic structural modulation of the surface begins mainly from 1000 K and a liquidized layer at the surface is formed as temperature increases. At the lower heating rate, when the temperature is 1090 K or higher, the melting of the whole particle happens and the interface between liquid and solid sweeps quickly inward from the surface (Figure S1 of the

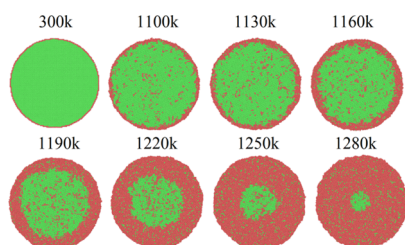


Figure 1. Snapshots of cross-section at different temperatures for a representative 20 nm Au particle. The atoms colored by green represent the local fcc crystalline structure as determined by PTM; the others that have non-fcc structural environment are colored red.

Supporting Information). Thus, for 20 nm gold particles, the premelting region is from 1000 to 1090 K and the melting point is approximately 1090 K.

For ultrafast heating rates, the concepts of a premelting layer and a single melting point should disappear.⁴¹ As shown in Figure 2a, the melting begins at 1000 K and finishes at 1300 K

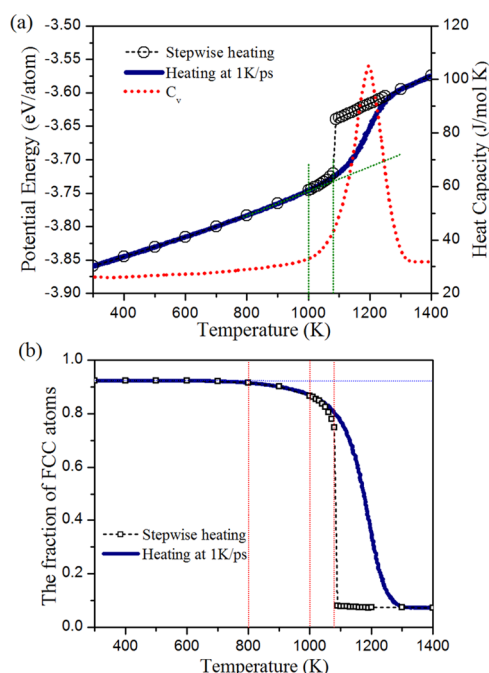


Figure 2. (a) Variations of potential energy (dark blue line) and heat capacity (red dotted line) with temperature for a representative 20 nm Au particle at the heating rate of 1 K/ps, and variation of potential energy (black circle) under stepwise heating, and (b) fraction of atoms that have local fcc crystalline structure as a function of temperature for the above Au nanoparticle, based on PTM.

at the heating rate of 1 K/ps based on the heat capacity curve. This is different from the melting point of about 1090 K observed from the curve of potential energy under the slow heating rate. With stepwise heating, there is a sharp step with the temperature, whereas the curve from the heating rate of 1 K/ps has a slow step.

A linear increase of potential energy implies a constant heat capacity consistent with Dulong–Petit behavior at high temperature. At the temperature of phase transition, the heat capacity will have a strong increase due to latent heat, which is spread out over a temperature range in nanoparticles. Under ultrafast heating rates, the slow nonlinear increase of potential

energy at about 1000 K with the increase of heat capacity implies the beginning of phase transition from solid to liquid. As seen in Figure 2, the peak in the heat capacity is asymmetric. The tail at the low temperature end of the peak indicates premelting near the surface.

The phase transition from solid to liquid can be also identified by the change of local atomic structure. PTM is a robust method for identifying the local crystalline structure of condensed phases.³⁴ It can separate the liquid atoms from the solid atoms with an fcc lattice according to the topology of local atomic environment. Here, this method was adopted to obtain the fraction of solid-like atoms. It is noticed that the atomic fraction of the surface layer does not change with temperature below 800 K and is approximately 7.6%. Based on the relation of $\Delta N/N = 3\Delta R/R$, where N is the number of gold atoms and R is the radius of nanoparticles, the width of the surface layer for 20 nm nanoparticles is approximately 2.5 Å.

Another effect is the fact that with the increase of temperature, the formation of defects in the interior of nanoparticles may occur. Below the premelting temperature, the probability of defect formation is small. Thus, the contribution of defects in the interior to the fraction of non-fcc atoms is small. Therefore, the increase of the fraction of non-fcc atoms is mainly from the contribution of near-surface layer melting. In Figure 2b, at 1000 K, the width of the surface layer obtained from the fraction of non-fcc atoms (8.65%) is about 4.5 Å. This value is similar to the lattice constant of bulk gold. With the increase of temperature to the premelting temperature of 1080 K, the width of surface layer becomes ~ 8.7 Å. The surface layer with liquid-like atoms at this temperature is called as premelting layer and the averaged width of 8.7 Å obtained here is similar to that in the report of Dai et al.²⁴ Above the premelting temperature, such as at 1090 K, the fraction of fcc atoms becomes very small at 0.084. This indicates melting of the full nanoparticle. In Figure S2 of the Supporting Information, from the change of fcc atomic fraction with time, the melting process at 1090 K is fast and the melting time is about 1.6 ns. However, if we adopt a high heating rate, such as 1 K/ps, the fraction of fcc atoms decreases slowly with the increase of temperature from 1080 K (Figure 2b), indicating melting over a large range of temperature, consistent with the heat capacity.

In order to analyze the local change of atomic structure in the melting process under a high heating rate, the CSP is useful. CSP is an effective way of measuring local ordering to interpret the nucleation of liquids.³⁵ The CSP of each atom is calculated through the formula, $CSP = \sum_{i=1,6} |R_i + R_{i+6}|^2$, where R_i and R_{i+6} are the vectors from the central atom to a pair of neighboring atoms with opposite directions corresponding to the six pairs of opposite nearest neighbors in the fcc lattice. It gives a measure of how far a structure is from being locally centrosymmetric. For an atom located in a perfect lattice, the value of CSP is zero or at finite temperature, near zero, reflecting small thermal fluctuations of the perfect lattice. Surfaces and defects generate large CSP values. This parameter can also distinguish the liquid atoms from solid atoms. For fcc gold, if the CSP value of one atom in the lattice is more than $8\text{--}10 \text{ \AA}^2$, this atom is considered to be in a liquid-like environment.²⁴

For analysis, it is helpful to separate a nanoparticle into a series of shells. We calculated the averaged CSP values of atoms in each shell. We plot the changes of CSP at fixed temperature point in Figure 3a as a function of distance based

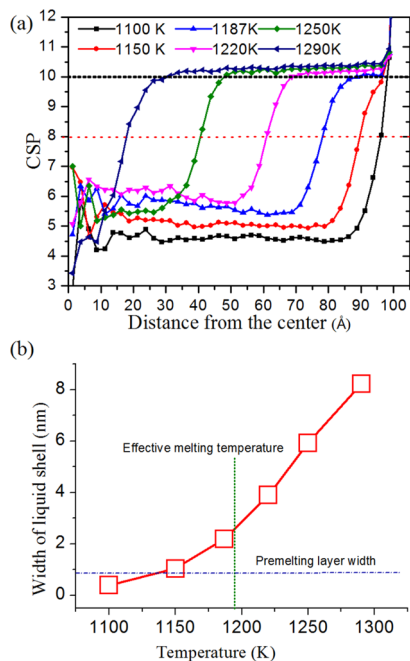


Figure 3. (a) CSP profile at different temperatures as a function of the distance from the center of 20 nm Au particle, and (b) width of liquid shell as a function of temperature. In (a), the upper flat black dotted line shows the cutoff, which is used to distinguish between solid and liquid atoms.

on shells. At 1100 K, the averaged CSP value of the interior solid atoms is about 4.6 \AA^2 and the averaged width of the liquid-like layer defined by $\text{CSP} = 8 \text{ \AA}^2$ is about 4 \AA . It is clear from the CSP values at different temperatures that the liquid region begins from the surface and expands to the inner region and that the width of the liquid shell increases with increasing temperature. In Figure 3b, we show the evolution of the width of the liquid shell with increasing temperature. The width increases nonlinearly with temperature and shows a slow increase at low temperature. From the peak position in heat capacity in Figure 2, the effective melting point is approximately 1195 K with a heating rate of 1 K/ps. At this temperature, the width of the liquid shell is about 2.6 nm, which is considerably larger than that (0.87 nm) of the premelting layer.

The melting of nanoparticles with different sizes from 6 to 24 nm was simulated with a heating rate of 1 K/ps. In Figure 4a, the average potential energy as the function of temperature for different particle sizes is shown. The potential energy per atom decreases with particle size at fixed temperature because of the decrease of surface/volume ratio. Correspondingly, the melting region is shifted to higher temperature with increasing particle size. This is related to the fact that the atomic coordination number reduction fosters the size dependency of the remelting and melting. Following the decrease of particle size, the atomic cohesive energy of surface atoms decreases due to the coordination number reduction, although the strengths of bonds between atoms near the surface gain because these bonds underwent spontaneous contraction. The specific heat is the first-order differentiation of the cohesive energy of the system and thus the melting temperature depends on the atomic cohesive energy. Therefore, it increases, following the decrease of surface/volume atomic ratio.

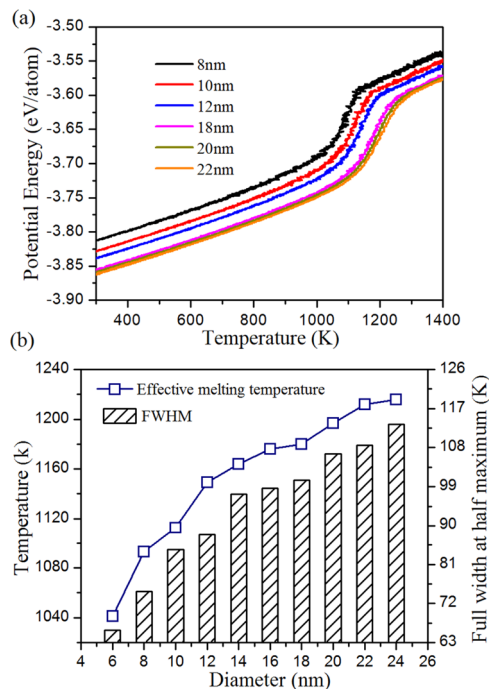


Figure 4. (a) Potential energies of six selected Au nanoparticles as the functions of temperature with continuous rapid heating at 1 K/ps, and (b) size-dependence of effective melting temperature, and fwhm from heat capacity curve.

As mentioned, the peak of the heat capacity can reveal the coexistence of solid and liquid in the melting process. Thus, the peak can identify the effective melting point, whereas the full width at half maximum (fwhm) can show the size of the coexistence region.⁴² In Figure 4b, the effective melting point and fwhm are shown as functions of particle size. The increase of melting point with the particle size is well known. It is interesting and somewhat unexpected that the fwhm value also increases with size in this size range. This no doubt reflects the fast heating rate and the finite time for the melted zone to propagate into the interior of the particle. Melting under a high heating rate is a thermokinetic process from the surface into the interior of the particle with the temperature increase. With increase of particle size, the process becomes slower and thus the temperature interval of solid–liquid coexistence becomes larger, as the fwhm indicates.

Because the melting process and effective melting temperature are sensitive to the heating rate,⁴³ melting under different heating rates was performed. The heat capacity for a particle size of 10 nm is shown in Figure 5a. With the increase of the heating rate, the peak for effective melting temperature is shifted to a higher temperature, whereas the fwhm value is increased noticeably. This is consistent with the discussion above. It is clear that the effective melting temperature under ultrafast heating rate is higher than the equilibrium melting point (1060 K for the size of 10 nm). Thus, with increasing heating rate, the fwhm increases as does the effective melting temperature.

In Figure 5b, the effective melting temperatures and fwhm values for three typical particle sizes (8, 10, and 12 nm) are shown. At the same heating rate, the fwhm value increases with particle size, similar to the behavior with heating rate of 1 K/ps. Regardless of the particle size, the effective melting temperature increases with the heating rate. In Figure 6, we

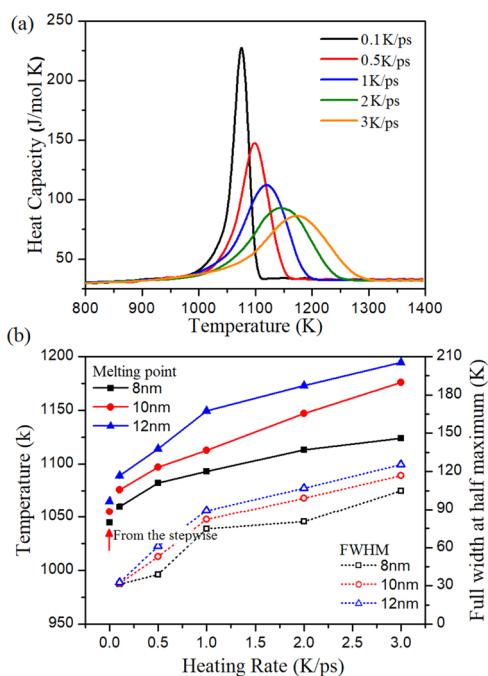


Figure 5. (a) Heat capacity for a 10 nm Au particle as a function of temperature under different heating rates, and (b) effective melting temperature and corresponding fwhm under different heating rates for 8, 10, and 12 nm Au particles.

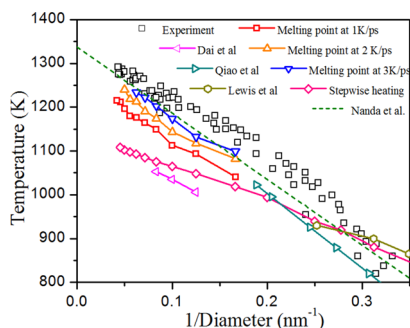


Figure 6. Simulated melting temperatures of Au nanoparticles with the inverse particle diameter, compared with previous simulations and experimental results for Au particles. The liquid drop model proposed by Nanda et al.⁴⁴ is also shown.

plot the effective melting temperature at heating rates of 1, 2, and 3 K/ps and the equilibrium melting temperature from stepwise heating as functions of the reciprocal of particle diameter ($1/D$), with the previous simulated results and experimental results as the reference. It is noticed that equilibrium melting temperature from our stepwise heating and from the work of Dai et al.²⁴ is clearly different from the change of melting temperature with $1/D$ and also from the existing experiment. The difference is mainly for particles with large size. From the discussion above, for larger particle size, the melting temperature is sensitive to the melting rate. Thus, we propose that the deviation of the melting temperature from the experiment for larger size is due to differences in the amount overheating because of different rates of temperature change. At the smaller particle size, the effect of overheating is not noticeable. Thus, it can be observed that the simulated results from the smaller size, such as 5–3.3 nm, including that

of our stepwise heating and from the works of Qiao et al.²⁸ and Lewis et al.²⁵ are similar to that of the experiment.

The effective melting temperature at the high heating rate follows approximately the rule of linearly decreasing relation of inverse diameter, similar to the experimental results for particle sizes larger than 5 nm. With the liquid drop model, the melting temperature of nanoparticles is connected to that of the bulk single crystal by the formula, $T_m = T_{mb}(1 - \beta/d)$, where the parameter β is related to the surface energy of the nanoparticle. With the value (1.1281 nm) of β from Nanda et al.,⁴⁴ the fit is shown as a dotted green line. All these are similar, although the melting temperature simulated by MD for a fixed particle size is a little less than that from the experiment. It is possible that the aggregation of particles and the substrate⁴⁵ in the experiment increase the measured melting temperature a little. It is also possible that the potential of gold in our simulation does not describe the surface atoms as well as the bulk. In addition, the effective melting temperature as we define may not exactly be the same as the way it is measured experimentally.

CONCLUSIONS

In summary, we explored the melting process and atomic mechanisms of nanoparticle gold at different heating rates by MD simulations with particle size from 6 to 24 nm. As in prior reports, there is a premelting layer near the surface. The width of the premelting layer in size of 20 nm is about 0.87 nm, similar to the observation of 8–12 nm in the report by Dai et al.²⁴ With ultrafast heating rates, the melting of nanoparticles becomes a process with solid–liquid coexistence in a large temperature interval, in addition to the premelting layer. Generally, as temperature increases, the interface between solid and liquid begins from the premelting layer and sweeps into the interior of the particle.

The melting point as defined by the heat capacity curve increases with particle size, whereas the width of the temperature interval is enlarged. From the changes with particle size and heating rate, it is inferred that the overheating effects in ultrafast heating conditions become more important for larger particles. The nucleation kinetics are mainly from the interface of solid and liquid which is initialized at the surface. It is also suggested that the melting point of nanoparticle gold in prior experiments is affected by overheating, as the change of melting temperature has a similar trend to that seen with high heating rates in the MD. From these results, the melting process of nanoparticles can be controlled by the heating rate and thus by the power density of lasers or/and electron beams.

ASSOCIATED CONTENT

Supporting Information

The Supporting Information is available free of charge at <https://pubs.acs.org/doi/10.1021/acs.jpcc.9b10769>.

Snapshots of cross section at 1080 K and 1090 K with heating times of 500 ps and 2000 ps for 20 nm Au particle; melting of 20 nm Au particle under stepwise heating; and heat capacity curves for 6–24 nm Au particle as functions of temperature at the heating rate of 1K/ps (PDF)

■ AUTHOR INFORMATION

Corresponding Author

Xiaofeng Fan – Key Laboratory of Automobile Materials (Jilin University), Ministry of Education, and College of Materials Science and Engineering, Jilin University, Changchun 130012, China; orcid.org/0000-0001-6288-4866; Phone: +86-159-4301-3494; Email: xffan@jlu.edu.cn

Authors

Jixing Chen – Key Laboratory of Automobile Materials (Jilin University), Ministry of Education, and College of Materials Science and Engineering, Jilin University, Changchun 130012, China

Jialin Liu – Key Laboratory of Automobile Materials (Jilin University), Ministry of Education, and College of Materials Science and Engineering, Jilin University, Changchun 130012, China

Changzhi Gu – Laboratory of Microfabrication, Beijing National Laboratory for Condensed Matter Physics, Institute of Physics, Chinese Academy of Sciences, Beijing 100190, China

Yunfeng Shi – Department of Material Science and Engineering, Rensselaer Polytechnic Institute, Troy, New York 12180, United States; orcid.org/0000-0003-1700-6049

David J. Singh – Department of Physics and Astronomy and Department of Chemistry, University of Missouri, Columbia, Missouri 65211-7010, United States; orcid.org/0000-0001-7750-1485

Weitao Zheng – Key Laboratory of Automobile Materials (Jilin University), Ministry of Education, and College of Materials Science and Engineering and State Key Laboratory of Automotive Simulation and Control, Jilin University, Changchun 130012, China

Complete contact information is available at:
<https://pubs.acs.org/10.1021/acs.jpcc.9b10769>

Notes

The authors declare no competing financial interest.

■ ACKNOWLEDGMENTS

The research was supported by the National Key R&D Program of China (Grant no. 2016YFA0200400) and the National Natural Science Foundation of China (Grant no. 51627805).

■ REFERENCES

- (1) Daniel, M.-C.; Astruc, D. Gold Nanoparticles: Assembly, Supramolecular Chemistry, Quantum-Size-Related Properties, and Applications toward Biology, Catalysis, and Nanotechnology. *Chem. Rev.* **2004**, *104*, 293–346.
- (2) Liu, X.; Wen, X.; Hoffmann, R. Surface activation of transition metal nanoparticles for heterogeneous catalysis: what we can learn from molecular dynamics. *ACS Catal.* **2018**, *8*, 3365–3375.
- (3) Couchman, P. R.; Jesser, W. A. Thermodynamic theory of size dependence of melting temperature in metals. *Nature* **1977**, *269*, 481–483.
- (4) Dick, K.; Dhanasekaran, T.; Zhang, Z.; Meisel, D. Size-Dependent Melting of Silica-Encapsulated Gold Nanoparticles. *J. Am. Chem. Soc.* **2002**, *124*, 2312–2317.
- (5) Levitas, V. I.; Samani, K. Size and mechanics effects in surface-induced melting of nanoparticles. *Nat. Commun.* **2011**, *2*, 284.
- (6) Sun, C. Q. Size dependence of nanostructures: Impact of bond order deficiency. *Prog. Solid State Chem.* **2007**, *35*, 1–159.
- (7) Sun, C. Q.; Wang, Y.; Tay, B. K. Correlation between the melting point of a nanosolid and the cohesive energy of a surface atom. *J. Phys. Chem. B* **2002**, *106*, 10701–10705.
- (8) Zhu, Y. F.; Lian, J. S.; Jiang, Q. Modeling of the melting point, Debye temperature, thermal expansion coefficient, and the specific heat of nanostructured materials. *J. Phys. Chem. C* **2009**, *113*, 16896–16900.
- (9) Liu, J.; Fan, X.; Shi, Y.; Singh, D. J.; Zheng, W. Melting of nanocrystalline gold. *J. Phys. Chem. C* **2019**, *123*, 907–914.
- (10) Buffat, P.; Borel, J.-P. Size effect on the melting temperature of gold particles. *Phys. Rev. A* **1976**, *13*, 2287–2298.
- (11) Lu, K.; Li, Y. Homogeneous nucleation catastrophe as a kinetic stability limit for superheated crystal. *Phys. Rev. Lett.* **1998**, *80*, 4474–4477.
- (12) Delogu, F. Mechanistic aspects of homogeneous and heterogeneous melting processes. *J. Phys. Chem. B* **2006**, *110*, 12645–12652.
- (13) Jin, Z. H.; Gumbsch, P.; Lu, K.; Ma, E. Melting mechanisms at the limit of superheating. *Phys. Rev. Lett.* **2001**, *87*, 055703.
- (14) Cahn, R. W. Melting and the surface. *Nature* **1986**, *323*, 668–669.
- (15) Alsayed, A. M.; Islam, M. F.; Zhang, J.; Collings, P. J.; Yodh, A. G. Premelting at defects within bulk colloidal crystals. *Science* **2005**, *309*, 1207–1210.
- (16) Peters, K. F.; Chung, Y.-W.; Cohen, J. B. Surface melting on small particles. *Appl. Phys. Lett.* **1997**, *71*, 2391–2393.
- (17) Wang, N.; Rokhlin, S. I.; Farson, D. F. Nonhomogeneous surface premelting of Au nanoparticles. *Nanotechnology* **2008**, *19*, 415701.
- (18) Pawlow, P. The dependency of the melting point on the surface energy of a solid body. *Z. Phys. Chem.* **1909**, *65*, 545–548.
- (19) Rie, E. Influence of surface tension on melting and freezing. *Z. Phys. Chem.* **1923**, *104*, 354–362.
- (20) Reiss, H.; Wilson, I. B. The effect of surface on melting point. *J. Colloid Sci.* **1948**, *3*, 551–561.
- (21) Xue, Y.; Zhao, Q.; Luan, C. The thermodynamic relations between the melting point and the size of crystals. *J. Colloid Interface Sci.* **2001**, *243*, 388–390.
- (22) Cui, Z.-X.; Zhao, M.-Z.; Lai, W.-P.; Xue, Y.-Q. Thermodynamics of size effect on phase transition temperatures of dispersed phases. *J. Phys. Chem. C* **2011**, *115*, 22796–22803.
- (23) Fu, Q.; Cui, Z.; Xue, Y.; Duan, H. Research of size- and shape-dependent thermodynamic properties of the actual melting process of nanoparticles. *J. Phys. Chem. C* **2018**, *122*, 15713–15722.
- (24) Dai, C.; Saidi, P.; Song, H.; Yao, Z.; Daymond, M. R.; Hoyt, J. J. A test of a phenomenological model of size dependent melting in Au nanoparticles. *Acta Mater.* **2017**, *136*, 11–20.
- (25) Lewis, L. J.; Jensen, P.; Barrat, J.-L. Melting, freezing, and coalescence of gold nanoclusters. *Phys. Rev. B: Condens. Matter Mater. Phys.* **1997**, *56*, 2248–2257.
- (26) Shim, J.-H.; Lee, B.-J.; Cho, Y. W. Thermal stability of unsupported gold nanoparticle: a molecular dynamics study. *Surf. Sci.* **2002**, *512*, 262–268.
- (27) Koga, K.; Ikeshoji, T.; Sugawara, K.-i. Size- and temperature-dependent structural transitions in gold nanoparticles. *Phys. Rev. Lett.* **2004**, *92*, 115507.
- (28) Qiao, Z.; Feng, H.; Zhou, J. Molecular dynamics simulations on the melting of gold nanoparticles. *Phase Transitions* **2013**, *87*, 59–70.
- (29) Ercolessi, F.; Andreoni, W.; Tosatti, E. Melting of small gold particles: mechanism and size effects. *Phys. Rev. Lett.* **1991**, *66*, 911–914.
- (30) Cleveland, C. L.; Luedtke, W. D.; Landman, U. Melting of gold clusters. *Phys. Rev. B: Condens. Matter Mater. Phys.* **1999**, *60*, S065–S077.
- (31) Ali, S.; Myasnichenko, V. S.; Neyts, E. C. Size-dependent strain and surface energies of gold nanoclusters. *Phys. Chem. Chem. Phys.* **2016**, *18*, 792–800.
- (32) Schlexer, P.; Andersen, A. B.; Sebok, B.; Chorkendorff, I.; Schiøtz, J.; Hansen, T. W. Size-dependence of the melting

temperature of individual Au nanoparticles. *Part. Part. Syst. Charact.* **2019**, *36*, 1800480.

(33) Vo, T. Q.; Kim, B. H. Molecular dynamics study of thermodynamic properties of nanoclusters for additive manufacturing. *Int. J. Precis. Eng. Manuf.-Green Technol.* **2017**, *4*, 301–306.

(34) Larsen, P. M.; Schmidt, S.; Schiøtz, J. Robust structural identification via polyhedral template matching. *Modell. Simul. Mater. Sci. Eng.* **2016**, *24*, 055007.

(35) Kelchner, C. L.; Plimpton, S. J.; Hamilton, J. C. Dislocation nucleation and defect structure during surface indentation. *Phys. Rev. B: Condens. Matter Mater. Phys.* **1998**, *58*, 11085–11088.

(36) Plimpton, S. Fast parallel algorithms for short-range molecular dynamics. *J. Comput. Phys.* **1995**, *117*, 1–19.

(37) Foiles, S. M.; Baskes, M. I.; Daw, M. S. Embedded-atom-method functions for the fcc metals Cu, Ag, Au, Ni, Pd, Pt, and their alloys. *Phys. Rev. B: Condens. Matter Mater. Phys.* **1986**, *33*, 7983–7991.

(38) Stukowski, A. Visualization and analysis of atomistic simulation data with OVITO-the Open Visualization Tool. *Modell. Simul. Mater. Sci. Eng.* **2010**, *18*, 015012.

(39) Evans, D. J.; Holian, B. L. The Nose-Hoover thermostat. *J. Chem. Phys.* **1985**, *83*, 4069–4074.

(40) Cahn, R. W. Melting from within. *Nature* **2001**, *413*, 582–583.

(41) Berry, R. S. Size is everything. *Nature* **1998**, *393*, 212–213.

(42) Zhang, M.; Efremov, M. Y.; Schiettekatte, F.; Olson, E. A.; Kwan, A. T.; Lai, S. L.; Wisleder, T.; Greene, J. E.; Allen, L. H. Size-dependent melting point depression of nanostructures: Nanocalorimetric measurements. *Phys. Rev. B: Condens. Matter Mater. Phys.* **2000**, *62*, 10548–10557.

(43) Hwang, Y. S.; Levitas, V. I. Superheating and melting within aluminum core-oxide shell nanoparticles for a broad range of heating rates: multiphysics phase field modeling. *Phys. Chem. Chem. Phys.* **2016**, *18*, 28835–28853.

(44) Nanda, K. K.; Sahu, S. N.; Behera, S. N. Liquid-drop model for the size-dependent melting of low-dimensional systems. *Phys. Rev. A* **2002**, *66*, 013208.

(45) Luo, W.; Su, K.; Li, K.; Liao, G.; Hu, N.; Jia, M. Substrate effect on the melting temperature of gold nanoparticles. *J. Chem. Phys.* **2012**, *136*, 234704.